# Modeling of quasi-three-level lasers and operation of cw Yb:YAG lasers

Takunori Taira, William M. Tulloch, and Robert L. Byer

We present modeling studies of quasi-three-level laser oscillators, the validity of which was revealed by Ti:$Al_2O_3$-pumped Yb:YAG laser experiments, and these results are shown to be in excellent agreement with the theory. As much as 75% slope efficiency was obtained with a hemispherical laser cavity. Previous modeling calculations of laser performance have been valid only for certain special cases, restricting application to $TEM_{00}$ Gaussian beam pumping and lasing profiles. This analysis may be applied to other longitudinally pumped quasi-three-level laser media in which the modes are not only $TEM_{00}$ Gaussian beams but also other higher-order transverse modes, including the top-hat pumping profile that can be used to model transverse pumping schemes. 

*Key words:* Quasi-three-level laser, Yb:YAG, mode-matching efficiency.

## 1. Introduction

Improved performance can be achieved by longitudinally pumping quasi-three-level lasers using diode lasers or other lasers instead of flash lamps because of the higher spatial and spectral brightness of the pump source. This higher brightness pumping has allowed room-temperature operation of quasi-three-level solid-state lasers that have significant population in the lower laser level, for example, the 946-nm $^4F_{3/2}$–$^4I_{9/2}$ transition of $Nd^{3+}$,[1] the 2080-nm $^5I_7$–$^5I_8$ transition of $Ho^{3+}$,[2] the 2020-nm $^3H_4$–$^3H_6$ transition of $Tm^{3+}$,[3] and the 1030-nm $^2F_{5/2}$–$^2F_{7/2}$ transition of $Yb^{3+}$.[4]

The trivalent ytterbium ion-doped YAG laser has several potential advantages compared with Nd:YAG. The advantages include low pump defect that results in a factor of 3 less heat generation, the potential for efficient $Q$-switched operation of Yb:YAG because of the 1-ms upper state lifetime, the lack of excited state absorption, the potential for efficient pumping because of higher doping in excess of 10 at. %, and ease of diode laser pumping that is due to broad absorption bands. In the last few years several reports have been devoted to the study of Yb:YAG lasers.[4–11]

In the past, a considerable number of studies have been made on modeling of longitudinally pumped lasers including the effect of overlap of the pump and laser field.[12,13] Several reports include the three-level absorption loss in the modeling calculations.[1,14] However, previous results apply only for the special case of $TEM_{00}$ Gaussian laser pumping and lasing profiles. The previous calculations do not consider the effects of non-Gaussian beam pumping.

We present the results of numerical modeling of the performance of a longitudinally pumped quasi-three-level laser, which was extended to include an arbitrary distribution of the pump and laser spatial modes. The threshold and slope efficiency are analyzed. To make the general concepts presented more concrete, we applied the results of the modeling to a Ti:$Al_2O_3$ laser-pumped Yb:YAG laser. The high slope efficiency and low threshold power were obtained for absorbed pump power with a hemispherical laser cavity and even higher efficiencies are predicted for diode pumping. These experimental results are shown to be in excellent agreement with the theory.

## 2. Theory

### A. Basic Model

There are a number of models of a quasi-three-level laser that have been made for longitudinally $TEM_{00}$ Gaussian beam pumping.[1,12–14] To extend the pre-

T. Taira is with the Department of Electrical and Electronics Engineering, Faculty of Engineering, Fukui University, 3-9-1 Bunkyo, Fukui 910, Japan. W. M. Tulloch and R. L. Byer are with the Edward L. Ginzton Laboratory, Stanford University, Stanford, California 94305.

Received 25 October 1995; revised manuscript received 10 April 1996.

0003-6935/97/091867-08$10.00/0

vious limit, we describe a formula of laser threshold and mode-coupling efficiency with spatial distribution functions as illustrated in the Appendix. For intrinsic cavity loss $L_i$ and output transmission $T$, we derive an equation for the threshold pump power of the laser:

$$P_{\text{th}} = \frac{h\nu_p (V_{\text{eff}}/l_c^*)}{2\eta_p \eta_a (f_1 + f_2)\sigma\tau_f}(L_i + T + 2N_1^0 \sigma l), \quad (1)$$

where $h\nu_p$ is the pump photon energy, $\eta_p$ is the pump quantum efficiency that includes the number of ions in the upper manifold created by one absorbed photon, $\eta_a$ is the absorption efficiency for pump power, $f_1$ is the fractional population in the lower laser level, $f_2$ is the fractional population in the upper laser level, $\sigma$ is the gain cross section, $\tau_f$ is the lifetime of the upper manifold, $\Delta N^0 = N_2^0 - N_1^0 \approx -N_1^0$ is the unpumped population-inversion density, $l$ is the length of the laser crystal, $l_c^* = l_c + (n - 1)l$ is the optical path length of the cavity, $n$ is the refractive index of the laser crystal, and $l_c$ is the geometric cavity length. The quantity $V_{\text{eff}}$ in Eq. (1) is the effective mode volume defined by

$$V_{\text{eff}} = 1/\iiint_{\text{crystal}} r_p(x, y, z)\phi_o(x, y, z)\mathrm{d}V, \quad (2)$$

where $r_p(x, y, z)$ is the spatial distribution of the pump energy and $\phi_o(x, y, z)$ is the spatial distribution of the laser photons.

A second question remains concerning the slope efficiency to calculate output power. The slope efficiency is given by Eq. (A14) in terms of the normalized parameters $F$ and $S$ as defined by Eqs. (A9) and (A10). In Eq. (A14) the normalized slope efficiency $\mathrm{d}S/\mathrm{d}F$ was introduced as a mode-coupling efficiency. Then, the mode-coupling efficiency is given by

$$\eta_m \equiv \frac{\mathrm{d}S}{\mathrm{d}F} = \frac{1 + B(l_c^*/nl)\iiint_{\text{crystal}} \dfrac{\phi_o(x, y, z)}{1 + S\phi_o(x, y, z)}\mathrm{d}V}{F\iiint_{\text{crystal}} \dfrac{[Fr_p(x, y, z) - B(l_c^*/nl)]\phi_o^2(x, y, z)}{[1 + S\phi_o(x, y, z)]^2}\mathrm{d}V}, \quad (3)$$

where $F$ is a normalized variable proportional to pump power, $S$ is a normalized variable proportional to internal laser power, and $B = 2N_1^0 \sigma l/\delta$ is the ratio of reabsorption loss to fixed cavity loss. The parameters $F$ and $S$ were previously treated by Moulton.[13] Fan and Byer included reabsorption loss in their rate equation analysis,[1] then parameter $B$ was introduced by Risk[14] with a similar formula. Although previously derived equations are limited to $\text{TEM}_{00}$ Gaussian mode distribution, Eq. (3) describes an arbitrary spatial distribution function.

### B. Gaussian Beam Pumping

Consider first the simplest case for which we assume that the transverse modes of the pump and laser beams are $\text{TEM}_{00}$ Gaussian beams with negligible diffraction in the gain medium. In this case we can use the variable $r$ as the transverse radial coordinate instead of $x$ and $y$. Then the normalized pump distribution function described in Eq. (A5) is given by

$$r_p(r, z) = \frac{2\alpha}{\pi w_p^2 \eta_a}\exp(-\alpha z)\exp\left(-\frac{2r^2}{w_p^2}\right) = \frac{\alpha l_c^*}{\eta_a a^2 C}\exp(-\alpha z)\exp(-\mathrm{x}), \quad (4)$$

and the normalized photon density described by Eq. (A6) is given by

$$\phi_o(r, z) = \frac{2}{\pi w_o^2 l_c^*}\exp\left(-\frac{2r^2}{w_o^2}\right) = \frac{\exp(-a^2\mathrm{x})}{C}, \quad (5)$$

where we have used the following parameters:

$$C = \pi w_o^2 l_c^*/2, \quad (6)$$

$$a = w_p/w_o, \quad (7)$$

$$\mathrm{x} = 2r^2/w_p^2, \quad (8)$$

where $C$ is the normalized factor for the photon cavity distribution function, $a$ is the ratio of pump and laser beam waists, and $\alpha$ is the absorption coefficient for pump wavelength. By substituting these distribution functions for Eqs. (1) and (3), it is easy to get threshold power and mode-matching efficiency. From Eq. (1), the lasing threshold in terms of incident pump power is

$$P_{\text{th}} = \frac{\pi h\nu_p w_o^2 (1 + a^2)}{4\eta_p \eta_a (f_1 + f_2)\sigma\tau_f}(L_i + T + 2N_1^0 \sigma l). \quad (9)$$

The mode-matching efficiency from Eq. (3) is given by

$$\eta_m = \frac{1 + \dfrac{B}{S/C}\ln(1 + S/C)}{(F/C)\displaystyle\int_0^\infty \frac{[(F/C)\exp(-\mathrm{x}) - Ba^2]}{[1 + (S/C)\exp(-a^2\mathrm{x})]^2}\exp(-2a^2\mathrm{x})\mathrm{d}\mathrm{x}}. \quad (10)$$

These are identical to the results in Refs. 13 and 14, although our model provides for a cavity length that may differ from the crystal length.

## 3. Experimental Results

### A. Spectroscopy of Yb:YAG

The energy level diagram of Yb:YAG is shown in Fig. 1.[8] $Yb^{3+}$ has a $4f^{13}$ shell that lacks one electron compared with a filled shell. There are only two manifolds, the ground $^2F_{7/2}$ state and an excited $^2F_{5/2}$ state, both of which are separated by approximately 10,000 $\text{cm}^{-1}$. Since only a single spectral band is available for pumping energy into the system, the

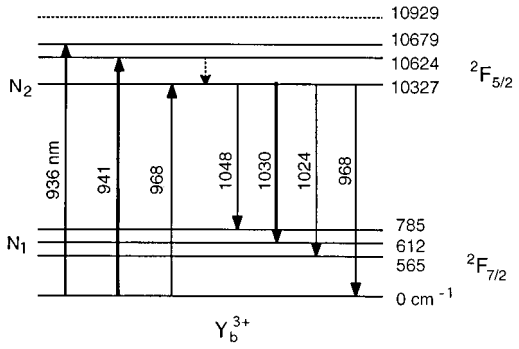


Fig. 1. Scheme of crystal splitting of the $^2F_{7/2}$ and $^2F_{5/2}$ levels of the $Yb^{3+}$ ion in a YAG laser.[8] The levels of the upper and lower manifolds and their energies are shown. The laser transition is noted by the heavy line. The populations of the upper and lower laser levels are given by $N_2$ and $N_1$, respectively.

previous use of white light from flash lamps rendered Yb impractical as a laser ion. Furthermore, because there are no additional $4f$ energy levels as in other trivalent rare earths, complications in laser media that result from concentration quenching, upconversion, and excited state absorption are not anticipated to affect laser performance.

As an example, 10-at. % $Yb^{3+}$-doped YAG has a total ion number of $N_0 = 13.8 \times 10^{20}$ ions/cm$^3$. The fractional population in the lower laser level is $f_1 = 0.046$, and the fractional population in the upper laser level is $f_2 = 0.70$. It is the fractional population of the lower laser level that leads to significant reabsorption loss. Figure 2 shows the $^2F_{5/2}$–$^2F_{7/2}$ absorption spectrum of $Yb^{3+}$ (Scientific Material Co.) taken at room temperature with a resolution of 0.1 nm. More accurate absorption coefficients, indicated by the circles, were measured with the Ti:$Al_2O_3$ laser. The strongest absorption line, $\alpha = 10.8$ cm$^{-1}$ for 10-at. % $Yb^{3+}$-doped crystal with a FWHM of 20.7 nm, is centered at 939.5 nm. Additional strong absorption lines were observed at 912 and 968 nm. These absorption spectral properties indicate that Yb:YAG is suitable for InGaAs diode laser pumping.

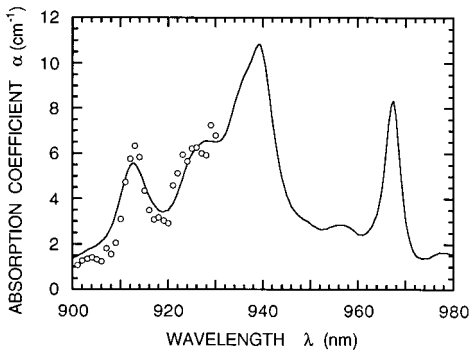


Fig. 2. Absorption spectra of 10-at. % Yb:YAG at room temperature with 0.1-nm resolution. The circles represent data points taken with a Ti:$Al_2O_3$ laser.

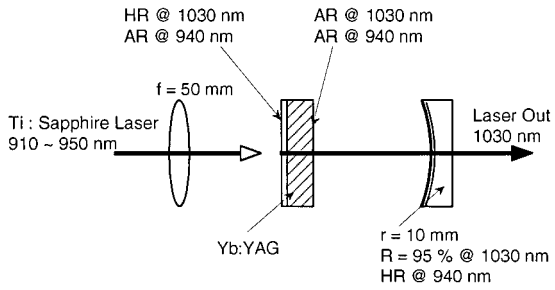


Fig. 3. Schematic of a Ti:$Al_2O_3$ laser pumped with a Yb:YAG short cavity laser.

### B. Characteristics of a Short-Cavity Yb:YAG Laser

A schematic diagram of the experimental apparatus is shown in Fig. 3. Typically longitudinally pumped laser configurations require an interface coated for high reflectivity (>99.9%) at the lasing wavelength and high transmission (>80%) at the pumping wavelength to couple the pump light into the laser cavity. For Yb:YAG the optimum pump wavelength of 940 nm is close to the 1030-nm lasing wavelength. Because of the small separation of these wavelengths, the reflectivity of the coupling interface is often difficult to control. For the Yb:YAG crystal used in this experiment, the coupling surface was one side of a flat–flat crystal. The transmission of this coating at 940 nm was >40%. At 913 nm the transmission of this coating increased to 95.5%, therefore these experiments were conducted using a Ti:$Al_2O_3$ pump laser tuned to 913 nm. Figure 2 shows an absorption coefficient measured at a Ti:$Al_2O_3$ wavelength of 913 nm for $\alpha = 6.3$ cm$^{-1}$. At 913 nm the Ti:$Al_2O_3$ laser delivered a maximum of 275 mW of $TEM_{00}$ cw pump power.

Two laser crystals were tested, which were polished flat–flat crystals with thicknesses of 0.5 and 1.1 mm, 4-mm diameter, and 10-at. % $Yb^{3+}$-doped YAG. One flat side of the crystal had the dielectric coating described above. The other side of the crystal was coated with an antireflection coating at both the pump and laser wavelengths. The cavity output coupler was a 10-mm radius of curvature mirror, coated for a reflectivity of 95% at 1030 nm and >99% at the pump wavelength. A 50-mm focal-length mode-matching lens was used to focus the pump beam to a diameter of 58 μm in the laser crystal.

Because of the quasi-three-level nature of the Yb:YAG laser, it is essential to achieve a high pump intensity and good mode matching between the pump and lasing modes. A hemispherical laser cavity was chosen because the short confocal length can be used to achieve tight focusing of the pump beam in the laser crystal. Figure 4 shows the threshold pump power and the output power of the Yb:YAG oscillator versus cavity length at a constant of 243.8 mW of pump power at 913 nm. It was observed that the minimum threshold power occurred with a cavity length of approximately 10 mm, which corresponds to the region where the

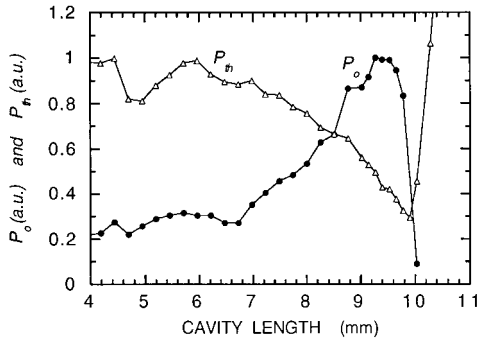


Fig. 4. Yb:YAG threshold power ($P_{\text{th}}$) and output power ($P_o$) versus the cavity length that results in a change of the laser mode spot size. For the output power measurement the 243.8-mW incident pump power was held constant at 913 nm.

laser cavity mode size is the smallest in the Yb:YAG crystal. However, the output power decreases sharply in this region because the small spot size of the laser mode leads to poor mode matching with the pump. In the cavity length range of 9.2–9.6 mm the output power is maximized, whereas the lowest threshold occurs at the longer cavity lengths. The results shown in Fig. 4 demonstrate the effect that mode matching and cavity optimization have on threshold and output power. The cavity length of 9.2 mm was selected for the remaining experiments to maximize output power and stability. The output beam was circularly symmetric with a divergence angle of 11.7 mrad.

Figure 5 shows the output power as a function of absorbed pump power for the two 1.1- and 0.5-mm long laser crystals that we tested. The minimum lasing threshold power was measured to be 21.1 mW with a slope efficiency of 75% for the 0.5-mm crystal. The maximum output power was 91.2 mW, demonstrated with the 1.1-mm crystal at an absorbed pump power of 197.6 mW. The solid curves in Fig. 5 represent the calculated values that we obtained when

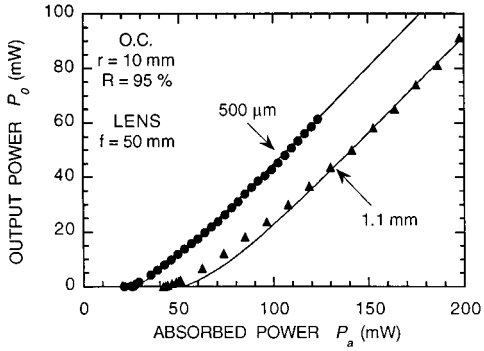


Fig. 5. Yb:YAG output power versus absorbed power at 913 nm. The solid curves represent numerically generated plots. In the calculation we used the values of $N_0 = 13.8 \times 10^{20}$ ions/cm$^3$, $\sigma = 3.3 \times 10^{-20}$ cm$^2$, $\tau_f = 0.951$ ms,[15] $\eta_p = 1.0$, $L_i = 0.6\%$, and $R_p = 100\%$.

we used the following pump distribution function:

$$r_p(r,z) = \frac{2\alpha}{\pi w_p^{\,2}\eta_a}\exp\left(-\frac{2r^2}{w_p^{\,2}}\right) \times \{\exp(-\alpha z) + \exp[-\alpha(z-2l)]\}$$

$$= \frac{\alpha l_c^{\,*}}{\eta_a a^2 C}\exp(-x)\{\exp(-\alpha z) + \exp[-\alpha(z-2l)]\}, \tag{11}$$

where

$$\eta_a = [1-\exp(-\alpha l)][1+R_p\exp(-\alpha l)], \tag{12}$$

where $\eta_a$ is the absorption efficiency for pump power and $R_p$ is the reflectivity of the pump wavelength at the internal crystal surface or external output mirror. In the calculation we used the following values: $\sigma = 3.3 \times 10^{-20}$ cm$^2$($\sigma_{\text{eff}} = f_2\sigma \sim 2.3 \times 10^{-20}$ cm$^2$), $\tau_f = 0.951$ ms,[15] $w_0 = 28$ μm, $\eta_p = 1.0$, $L_i = 1.0\%$, and $R_p = 100\%$.

There is good agreement between the experimental and calculated values, although the calculated thresholds are slightly higher than the experimental values. The calculation utilizes $\text{TEM}_{00}$ Gaussian mode beam distributions for both the pump and laser modes.

## 4. Discussion

### A. Top-Hat Beam Pumping

Here we assume the semiideal case, Gaussian laser beam output, and the top-hat beam pump. The pump distribution function is given by

$$r_p(r,z) = \frac{\alpha}{\pi w_p^{\,2}\eta_a}\exp(-\alpha z) = \frac{\alpha l_c^{\,*}}{2\eta_a a^2 C}\exp(-\alpha z), \quad r \le w_p, \tag{13a}$$

$$= 0 \qquad r > w_p, \tag{13b}$$

where $w_p$ is the beam radius, the pump intensity of the inside of $w_p$ is unity, and outside of $w_p$ it is zero. As mentioned above, $F/C$ is given by

$$\frac{F}{C} = \frac{2\left[1+\dfrac{B}{S/C}\ln(1+S/C)\right]}{\displaystyle\int_0^2 \frac{\exp(-a^2x)}{1+(S/C)\exp(-a^2x)}dx}. \tag{14}$$

At near threshold the mode-matching efficiency is reduced to

$$\frac{F_{\text{th}}}{C} = \frac{2a^2(1+B)}{1-\exp(-2a^2)}. \tag{15}$$

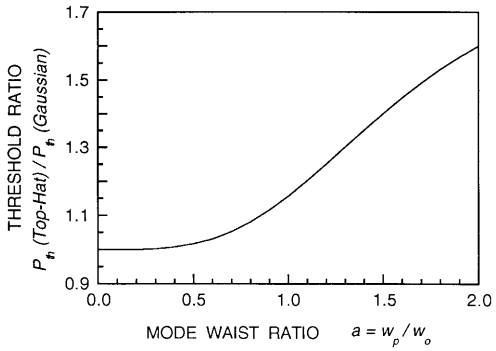


Fig. 6. Calculated threshold ratio of the top-hat to the Gaussian beam pumping scheme. As $a$ approaches 0 both values become equal. For $a \neq 0$, the threshold of the top-hat pumping scheme is higher than that for the Gaussian beam. (The maximum value is 2.)

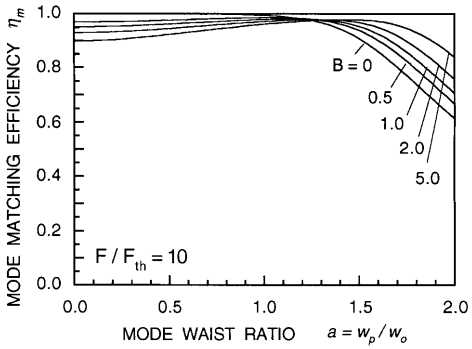


Fig. 7. Numerically generated plots of the mode-matching efficiency $\eta_m = dS/dF$ for the top-hat pump condition as a function of $a = w_p/w_o$ for different values of $B$, $F/F_{th} = 10$. It is obvious that at a much higher pumping region ($F/F_{th} > 5$) the mode-matching efficiency of the top-hat beam pumping will increase and perform well compared with the Gaussian beam pumping scheme.

From Eq. (15) the threshold is given by

$$P_{th} = \frac{\pi h \nu_p {w_o}^2}{4\eta_p \eta_a (f_1 + f_2)\sigma\tau_f}\left[\frac{2a^2}{1 - \exp(2a^2)}\right] \times (L_i + T + 2N_1{}^0 \sigma l). \quad (16)$$

The threshold power ratio of the top-hat to Gaussian pumping geometry is given by

$$\frac{P_{th}\,(\text{top-hat})}{P_{th}\,(\text{Gaussian})} = \frac{2a^2}{(1 + a^2)[1 - \exp(2a^2)]} \quad (17)$$

and is shown in Fig. 6. At the pump spot size ratio $a = 0$, the threshold power is equal to the Gaussian pumping case. It is clear that the threshold ratio is increased from 1 to 2 with the factor of $a$. In fact, the threshold power increases rapidly with spot size. This result indicates that the Gaussian pumping geometry has advantages in the low pumping region.

By substituting the distribution function Eqs. (13) into Eq. (3), we obtained the mode-matching efficiency formula as follows:

$$\eta_m = \frac{2\left[1 + \frac{B}{S/C}\ln(1 + S/C)\right]}{(F/C)\left\{(F/C)\int_0^2 \frac{\exp(-2a^2 x)}{[1 + (S/C)\exp(-a^2 x)]^2}\,dx - 2Ba^2\int_0^\infty \frac{\exp(-2a^2 x)}{[1 + (S/C)\exp(-a^2 x)]^2}\,dx\right\}}. \quad (18)$$

In addition, near threshold the mode-matching efficiency is given by

$$\eta_m|_{S\to 0} = \left[\frac{1 - \exp(-2a^2)}{a^2}\right]\frac{1}{1 + (1 + B)\exp(-2a^2)}. \quad (19)$$

Numerically generated plots of the normalized slope efficiency are shown in Fig. 7; i.e., mode-matching efficiency $\eta_m = dS/dF$ for the top-hat pump condition as a function of mode waist ratio $a = w_p/w_o$ for different values of $B$ with $F/F_{th} = 10$. The calculated results are similar to a $TEM_{00}$ Gaussian mode case. As a result, the optimum value of the mode waist ratio $a$ is 1.2–1.3 for top-hat mode distribution. Figure 8 shows calculated results of the mode-matching results as a function of pumping power ratio with $a = 1.2$. Although the laser threshold for the Gaussian pumping geometry is lower than the top-hat beam pumping, the top-hat beam pumping rapidly saturates the reabsorption loss for the mode-matching efficiency. Reflection on some of these facts indicates that the top-hat beam pumping condition is advantageous for a high power laser.

### B. Side Pumping

If we suppose a transverse pumping scheme, it would be necessary for us to change the pump distribution function as follows:

$$r_p(r, z) = \frac{2}{\pi {w_p}^2 \eta_a}\exp\left(-\frac{2r^2}{{w_p}^2}\right) = \frac{\exp(-x)}{a^2 C} \quad \text{(for Gaussian)}, \quad (20)$$

$$r_p(r, z) = \frac{1}{\pi {w_p}^2 l} = \frac{1}{2a^2 C}, \quad r \le w_p \quad \text{(for top-hat)}. \quad (21)$$

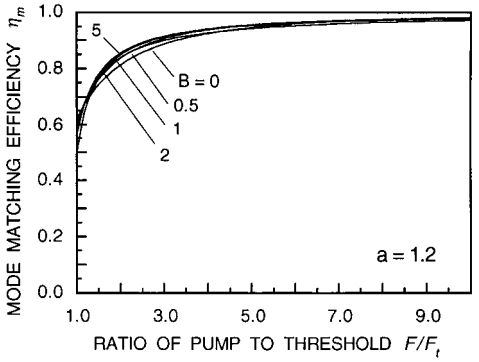


Fig. 8. Calculation of the mode-matching results as a function of pumping power ratio for top-hat beam pumping: $a = 1.2$.

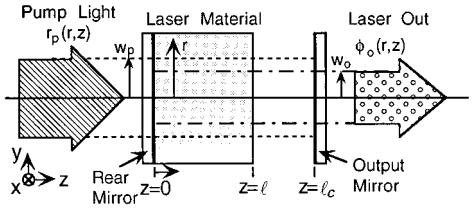


Fig. 9. Schematic of a longitudinally pumped solid-state laser.

Finally, we obtain the same equations for absorbed power instead of incident power. For that reason,the above analysis may be applied to the transverse pumping model.

## 5. Conclusion

We have presented an analysis for the performance of longitudinally pumped quasi-three-level laser oscillators with particular attention given to the Yb:YAG laser. This model can be applied to other quasi-three-level laser sources as well as more traditional four-level systems. With this model we predict high slope efficiencies from a quasi-three-level Yb:YAG laser oscillator, which we confirmed by experimental results that were demonstrated with a Ti:$Al_2O_3$ laser pumped, short cavity, Yb:YAG laser. The laser cavity length was optimized to demonstrate low thresholds and high slope efficiency operation. A maximum slope efficiency of 75% was achieved.

The model provides the capability of using a variety of pumping and lasing transverse modes and can be extended to side-pumped systems by a first-order approximation of a top-hat pump beam. The flexibility of this model enables the design of a second-generation diode-pumped Yb:YAG laser system to operate at high powers for applications such as a gravitational wave interferometer.

## Appendix

By starting with rate equations that describe photon density and population inversion in the steady-state case of a laser cavity, one can model the behavior of the laser with reabsorption loss. Figure 9 shows a schematic of the pump and laser geometry. The spatial distribution of the pump energy is given by $r_p(x, y, z)$ and the spatial distribution of the laser photons is given by $\phi_o(x, y, z)$. Here the $x$ and $y$ axes are the transverse coordinates, and $z$ is the coordinate along the axis of the laser. If it is unnecessary to consider the depletion of the ground-state population, the laser rate equations for population inversion density $\Delta N(x, y, z) = N_2(x, y, z) - N_1(x, y, z)$ and the total laser photon number in the cavity can be written as[1,12,14]

$$\frac{d\Delta N(x,y,z)}{dt} = 0 = (f_1 + f_2)Rr_p(x,y,z) - \frac{\Delta N(x,y,z) - \Delta N^0}{\tau_f} - \frac{(f_1 + f_2)c\sigma\Delta N(x,y,z)}{n}\Phi\phi_o(x,y,z), \tag{A1}$$

$$\frac{d\Phi}{dt} = 0 = \frac{c\sigma}{n}\iiint_{\text{crystal}} \Delta N(x,y,z)\Phi\phi_o(x,y,z)dV - \frac{\Phi}{\tau_c}, \tag{A2}$$

where $\Delta N^0 = N_2{}^0 - N_1{}^0 \approx -N_1{}^0$ is the unpumped population-inversion density, $\tau_f$ is the lifetime of the upper manifold, $c$ is the speed of light in vacuum, $\sigma$ is the gain cross section, $n$ is the refractive index of the laser medium, $\tau_c = 2l_c^*/c\delta$ is the cold-cavity lifetime, $l_c^* = l_c + (n - 1)l$ is the optical path length of the cavity, $\delta = L_i + T$ is the round-trip loss, $L_i$ is the intrinsic cavity loss, and $T$ is the output transmission. The diffusion of the excited state ions is neglected. $R$ is the total pump rate given by

$$R = \frac{\eta_p\eta_a P_p}{h\nu_p}, \tag{A3}$$

where $P_p$ is the incident pump power, $h\nu_p$ is the pump photon energy, $\eta_p$ is the pump quantum efficiency, which is the number of ions in the upper manifold created by one absorbed photon, and $\eta_a$ is the fraction of incident pump power absorbed in a crystal of length $l$. $\Phi$ is the total number of photons in the cavity given by

$$\Phi = \frac{2l_c^* P_o}{cTh\nu_L}, \tag{A4}$$

where $P_o$ is the laser output power from the cavity and $h\nu_L$ is the laser photon energy. The normalized distribution function of $r_p(x, y, z)$ is taken over the crystal, i.e.,

$$\iiint_{\text{crystal}} r_p(x,y,z)dV = \int_{x=0}^{\infty}\int_{y=0}^{\infty}\int_{z=0}^{l} r_p(x,y,z)dxdydz = 1, \tag{A5}$$

whereas the normalization of $\phi_o(x, y, z)$ is taken over the entire cavity, i.e.,

$$\iiint_{\text{cavity}} \phi_o(x, y, z)\mathrm{d}V = \int_{x=0}^{\infty}\int_{y=0}^{\infty}\left[\int_0^l n\phi_o(x, y, z)\mathrm{d}z + \int_l^{l_c} \phi_o(x, y, z)\mathrm{d}z\right]\mathrm{d}x\mathrm{d}y = 1. \tag{A6}$$

Note that the photon density in the active material with refractive index $n$ is $n$ times higher than that of free space. From Eq. (A1), the population-inversion density is given by

$$\Delta N(x, y, z) = \frac{(f_1 + f_2)\tau_f R r_p(x, y, z) - N_1{}^0}{1 + \dfrac{(f_1 + f_2)c\sigma\tau_f}{n}\Phi\phi_o(x, y, z)}. \tag{A7}$$

Below threshold, the inversion density is given by $\Phi = 0$. Equation (A7) indicates that the unpumped and the below-threshold regions exhibit reabsorption loss and the three-level-laser medium may act as a spatial filter.[16]

The spatial distribution of the population inversion can change under saturation conditions. The population-inversion density given in Eq. (A7) can be substituted directly into Eq. (A2) to obtain an implicit relationship between the pumping rate $R$ and the total laser cavity photon number $\Phi$:

$$\frac{2\sigma l_c{}^*}{n}\iiint_{\text{crystal}} \frac{(f_1 + f_2)\tau_f R r_p(x, y, z) - N_1{}^0}{1 + \dfrac{(f_1 + f_2)c\sigma\tau_f}{n}\Phi\phi_o(x, y, z)} \times \phi_o(x, y, z)\mathrm{d}V = \delta. \tag{A8}$$

This implicit relationship can be solved to determine the threshold and the slope efficiency of the laser. This equation indicates that the intrinsic gain, which includes the pumped gain and reabsorption loss, is equal to the round-trip loss that includes the intrinsic cavity loss and output transmission. To solve Eq. (A8) it is necessary to define the following parameters:

$$F = \frac{2(f_1 + f_2)\sigma\tau_f l_c{}^*}{n\delta} R, \tag{A9}$$

$$S = \frac{(f_1 + f_2)c\sigma\tau_f}{n}\Phi, \tag{A10}$$

$$B = \frac{2N_1{}^0\sigma l}{\delta}. \tag{A11}$$

Substituting Eqs. (A9)–(A11) into Eq. (A8) we obtain

$$F = \frac{1 + B(l_c{}^*/nl)\displaystyle\iiint_{\text{crystal}} \frac{\phi_o(x, y, z)}{1 + S\phi_o(x, y, z)}\mathrm{d}V}{\displaystyle\iiint_{\text{crystal}} \frac{r_p(x, y, z)\phi_o(x, y, z)}{1 + S\phi_o(x, y, z)}\mathrm{d}V}, \tag{A12}$$

where $F$ is a normalized variable proportional to pump power, $S$ is a normalized variable proportional to internal laser power, and $B$ is the ratio of reabsorption loss to fixed cavity loss. The parameters $F$ and $S$ were previously treated by Moulton.[13] Fan and Byer included reabsorption loss in their rate equation analysis,[1] then parameter $B$ was introduced by Risk[14] with a similar formula. Although previously derived equations are limited to $\mathrm{TEM}_{00}$ Gaussian mode distribution, Eq. (A12) describes an arbitrary spatial distribution function.

Equation (A12) can be solved to determine the threshold of the laser ($S = 0$) and the slope efficiency of the laser above threshold ($S > 0$). A formula for the laser threshold can be obtained from Eq. (A12) by letting $S = 0$. If the losses in the laser cavity are small, we can rewrite Eq. (A12) as

$$F_{\text{th}} = \frac{1 + B(l_c{}^*/nl)\displaystyle\iiint_{\text{crystal}} \phi_o(x, y, z)\mathrm{d}V}{\displaystyle\iiint_{\text{crystal}} r_p(x, y, z)\phi_o(x, y, z)\mathrm{d}V} = \left[1 + B(l_c{}^*/nl)\iiint_{\text{crystal}} \phi_o(x, y, z)\mathrm{d}V\right]V_{\text{eff}}, \tag{A13}$$

where we have used the effective mode volume as defined by Eq. (2), which was introduced by Kubodera and Otsuka.[12] Finally we obtained the threshold pump power of the laser by substituting Eq. (A3) into Eq. (A9) and solving for $P_{\text{th}}$ with respect to Eq. (1).

The slope efficiency of the laser is defined as a differential output power with pump power

$$\eta_s = \frac{\mathrm{d}P_o}{\mathrm{d}P_p} = \eta_p\eta_a\frac{T}{\delta}\frac{\nu_L}{\nu_P}\frac{\mathrm{d}S}{\mathrm{d}F}, \tag{A14}$$

where $\mathrm{d}S/\mathrm{d}F$ is the normalized slope efficiency that has been used by Moulton[13] and Risk.[14] Substitution of Eqs. (A9)–(A11) into Eq. (A8) and differentiation with respect to the normalized photon number $S$, results in the normalized slope efficiency defined in Eq. (3), where $F$ relates to $S$ by Eq. (A12). To make an approximate calculation, note that the formula for times when the slope efficiency near threshold ($S \rightarrow$

0) and the four-level laser system ($B = 0$) are

$$\left.\frac{dS}{dF}\right|_{S,B\to 0} = \frac{\left[\iiint_{\text{crystal}} r_p(x,y,z)\phi_o(x,y,z)dV\right]^2}{\iiint_{\text{crystal}} r_p(x,y,z)\phi_o{}^2(x,y,z)dV}. \quad \text{(A15)}$$

The left-hand side of Eq. (A15) is the same as the coupling efficiency between the pump and laser beams as outlined by Kubodera and Otsuka.[12] The value of $dS/dF$ can be considered as the mode-matching efficiency between the pump and laser beams, taking into account the reabsorption losses and saturation factor. Because Eqs. (A13) and (3) include the flexibility of arbitrary distribution functions for the pump and laser modes, $r_p(x, y, z)$ and $\phi_o(x, y, z)$, it is easy to calculate the threshold power and slope efficiency for a variety of configurations, i.e., the pump and laser cavity modes are not limited to $TEM_{00}$ Gaussian beams but can also be modeled as a higher transverse mode or more complicated functions.

We acknowledge the support of the National Science Foundation and the technical discussions with M. Fejer and A. Alfrey of Stanford University, and T. Y. Fan of the MIT Lincoln Laboratory.

## References

1. T. Y. Fan and R. L. Byer, "Modeling and CW operation of a quasi-three-level 946 nm Nd:YAG laser," IEEE J. Quantum Electron. **QE-23,** 605–612 (1987).
2. P. J. M. Suni and S. W. Henderson, "1-mJ/pulse Tm:YAG laser pumped by a 3-W diode laser," Opt. Lett. **16,** 817–819 (1991).
3. T. Y. Fan, G. Huber, R. L. Byer, and P. Mitzscherlich, "Spectroscopy and diode laser-pumped operation of TmHo:YAG," IEEE J. Quantum Electron. **QE-24,** 924–933 (1988).
4. P. Lacovara, H. K. Choi, C. A. Wang, R. L. Aggarwal, and T. Y. Fan, "Room-temperature diode-pumped Yb:YAG laser," Opt. Lett. **16,** 1089–1091 (1991).
5. T. Y. Fan, "Optimizing the efficiency and stored energy in quasi-three-level laser," IEEE J. Quantum Electron. **28,** 2692–2697 (1992).
6. T. Y. Fan, "Heat generation in Nd:YAG and Yb:YAG," IEEE J. Quantum Electron. **29,** 1457–1459 (1993).
7. T. Y. Fan, S. Klunk, and G. Henein, "Diode-pumped *Q*-switched Yb:YAG laser," Opt. Lett. **18,** 423–425 (1993).
8. W. F. Krupke and L. L. Chase, "Ground-state depleted solid-state lasers: principles, characteristics, and scaling," Opt. Quantum Electron. **22,** S1–S22 (1990).
9. L. D. DeLoach, S. A. Payne, L. L. Chase, L. K. Smith, W. L. Kway, and W. F. Krupke, "Evaluation of absorption and emission properties of $Yb^{3+}$ doped crystals for laser applications," IEEE J. Quantum Electron. **29,** 1179–1191 (1993).
10. D. Pelenc, B. Chambaz, I. Chartier, B. Ferrand, C. Wyon, D. P. Shepherd, D. C. Hanna, A. C. Large, and A. C. Tropper, "High slope efficiency and low-threshold in a diode-pumped epitaxially grown Yb:YAG waveguide laser," Opt. Commun. **115,** 491–497 (1995).
11. A. Giesen, H. Hugel, A. Voss, K. Witting, U. Brauch, and H. Opower, "Scalable concept for diode-pumped high-power solid-state lasers," Appl. Phys. B **58,** 365–372 (1994).
12. K. Kubodera and K. Otsuka, "Single-transverse-mode $LiNdP_4O_{12}$ slab waveguide laser," J. Appl. Phys. **50,** 653–659 (1979).
13. P. F. Moulton, "An investigation of the Co:$MgF_2$ laser system," IEEE J. Quantum Electron. **21,** 1582–1595 (1985).
14. W. P. Risk, "Modeling of longitudinally pumped solid-state lasers exhibiting reabsorption losses," J. Opt. Soc. Am. B **5,** 1412–1423 (1988).
15. D. S. Sumida and T. Y. Fan, "Effect of radiation trapping on fluorescence lifetime and emission cross section measurements in solid-state laser media," Opt. Lett. **19,** 1343–1345 (1994).
16. T. Y. Fan, "Aperture guiding in quasi-three-level lasers," Opt. Lett. **19,** 554–556 (1994).